Interlevel Cascade Transition in Electrically Confined Quantum Wire Arrays

Wei Wu, Iman Hassani, and Hooman Mohseni*

Bio-inspired Sensors and Optoelectronics Laboratory (BISOL), Department of Electrical Engineering and Computer Science, Northwestern University, Evanston, Illinois 60208, United States

ABSTRACT Vertical stacks of electrically confined quantum wires were demonstrated in devices with large areas. Multiple current plateaus and strong differential conductance oscillations were observed at above liquid nitrogen temperatures because of interlevel cascade transition of carriers. Our simulation results for charge transport, as well as interlevel infrared photoresponse red-shift, due to lateral electric field confinement show good agreement with experimental data.

KEYWORDS: quantum structures · quantum wires · electrical confinement · interlevel · current plateaus · conduction oscillations

Quantum structures such as quantum dots (QDs) or wires (QWRs) have unique electronic and optical properties because of their multidimensional quantum confinement.[1] For example, strongly nonlinear transport characteristics, such as Coulomb blockade and resonant tunneling, have been demonstrated in the low-dimensional structures.[2−5] A decrease of the nonradiative losses due to the reduced electron-longitudinal-optical-phonon (LO-phonon) scattering has also been shown in the quantum structures.[6,7] Because of their unique properties, quantum structures are very attractive for optoelectronic device applications.[8−13] The transport and photonic phenomena studies of quantum structures have resulted in the development of tunneling injection quantum dot lasers and quantum wire intersubband emitters and photodetectors.[14−17] Recently, the interlevel/intersublevel cascade transitions of carriers have also been studied and developed for terahertz quantum cascade laser applications.[9,13,18] Most experimental realizations of the quantum structures rely on physical material removal (etching), which produces inevitable structural damage and device performance degradation.[17,19] Other methods, such as self-assembled growth, have addressed this issue but result in limited size uniformity over large areas.[20,21] Electrical confinement methods, such as using multiple top metal gates to deplete the two-dimensional electron gas in a heterostructure, have been widely used to form low-dimensional structures.[22−24] However, the geometry of these ultrathin devices renders extremely small overlap to optical modes within the visible/infrared bands, and hence they have been mainly used for lateral transport studies and electronic devices. Forming vertical stacks of uniform quantum structures is an attractive method to increase the interaction between photons and electrons.[25] Nonetheless, electronic vertical transport and carrier transitions in stacked QWRs are much less studied compared with its potential applications.[25,26] For example, the resonant tunneling and the reduced nonradiative losses in quantum wires could lead to development of novel terahertz emitters and detectors working at high temperatures.[14,27,28]

Here we report on a novel method of forming vertical stacks of QWRs based on an external electric field confinement of carriers in quantum wells and experimentally study the transport property of the structure at different temperatures. Using a distributed metal gate, we induce electrical depletion in the quantum wells around a nanoridge of 200 nm width. This produces a strong lateral confinement, in addition to the vertical confinement produced by the heterojunctions, to create tunable QWRs. The schematic of the proposed device structure is shown in Figure 1. The long nanoridge arrays of highly doped $In_{0.53}Ga_{0.47}As$ are used to connect the top contacts of all quantum wires and to produce an undercut in the lower layer of InP, which can help disconnect the gate from the top contacts. With a negative gate voltage, the generated electric field can effectively deplete the electrons from the areas below the nanoridges

* Address correspondence to hmohseni@northwestern.edu.

Received for review July 1, 2011 and accepted August 21, 2011.

Published online August 21, 2011
10.1021/nn202440j

and form quantum confinement in the lateral direction. On the basis of this idea, we successfully realize the QWR devices experimentally and present the electrical and optical verification of this lateral confinement. Multiple current plateaus and strong differential conduction oscillations up to 123 K were observed. Our modeling shows that resonant tunneling between the energy states in different quantum wells produced by electrical confinement is responsible for this behavior. Also, the model predicts the measured red-shift of the peak photoresponse accurately.

DEVICE FABRICATION

The quantum well structure was grown by metal-organic chemical vapor deposition (MOCVD) on a semi-insulation (100) InP substrate. The active region, sandwiched between 500 nm n-doped $In_{0.53}Ga_{0.47}As$ (doping concentration 10^{18} cm^{-3}) at the bottom and 40 nm at the top, consists of 8 periods of 50 nm InP barriers and 5.6 nm n-doped $In_{0.53}Ga_{0.47}As$ wells with a nominal doping concentration of 2.5×10^{17} cm^{-3}. The thickness of the first InP barrier from the top is 100 nm and is used for formation of the undercut. Because of the good adhesion between epitaxial layers of $In_{0.53}Ga_{0.47}As$ and InP, $In_{0.53}Ga_{0.47}As$ nanoridges were used as masks to wet etch the InP layer below and form the undercut shape along the $\langle 01\bar{1} \rangle$ direction.[29] A thin dielectric layer of SiO_2 was deposited before the deposition of the gate layer. The periodic highly doped $In_{0.53}Ga_{0.47}As$ nanoridge arrays of 200 nm width and 1 μm periodicity were formed by electron beam lithography and subsequent reactive ion etching (RIE) of $In_{0.53}Ga_{0.47}As$. Within a device, all nanoridges were connected at one end, and all the gate contacts were connected at the other end.

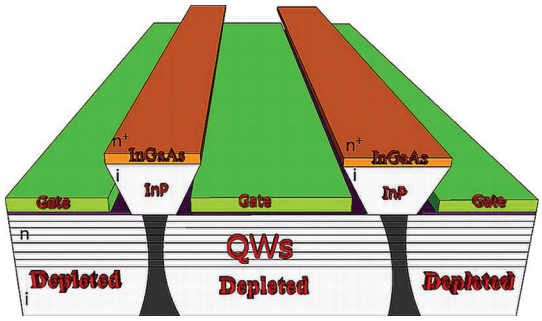

Figure 1. Quantum wire device structure formed by electrical confinement in quantum wells.

Figure 2 shows the major fabrication sequence for the electrically confined QWR device. First, a HSQ e-beam resist was patterned on top of the quantum wells sample by electron beam lithography to form periodic nanoridge arrays, and the nanoridges were used as masks to transfer the patterns to the $In_{0.53}Ga_{0.47}As$ layer (Figure 2a). Second, a SiO_2 layer was deposited using plasma-enhanced chemical vapor deposition (PECVD) and patterned so that it was used as a mask to etch the whole QW active layer until reaching the bottom doped $In_{0.53}Ga_{0.47}As$ contact layer

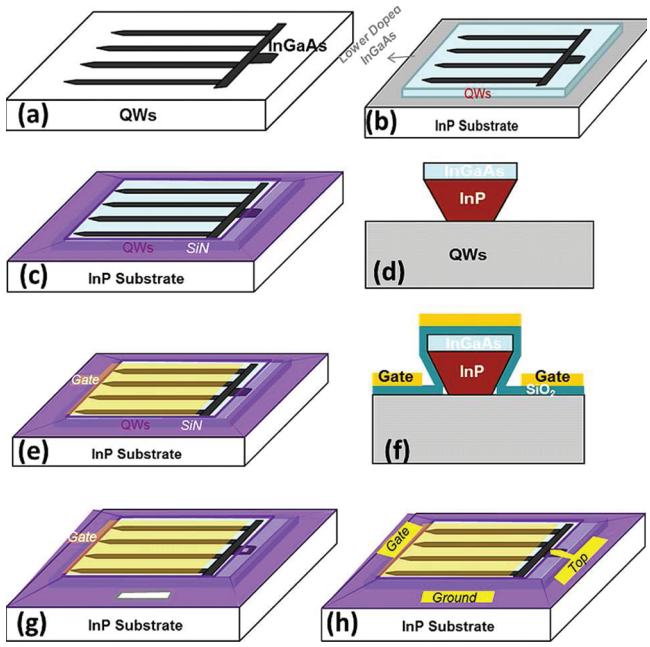

Figure 2. Schematics of major device fabrication steps: (a) e-beam lithography produces InGaAs nanoridge arrays, (b) separate mesas with InGaAs nanoridges on the top were formed, (c) a thick Si_xN_y layer was deposited to passivate the etched surface, and an opening was formed in the Si_xN_y layer, (d) side view of the InGaAs and InP layers normal to the nanoridges after wet etching of InP, (e) Ti/Au gate contact layer was deposited and patterned after SiO_2 dielectric deposited, (f) side view of the device after SiO_2 dielectric and gate contact layers, (g) a small channel was opened on the top metal contact, and an opening was formed for the ground contacts, (h) final device structure after top, gate, and ground metal contacts were deposited and patterned.

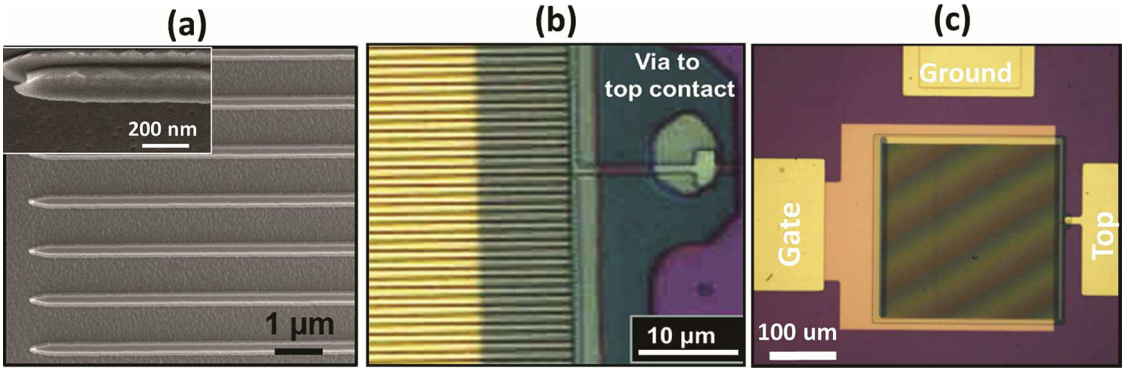

Figure 3. (a) SEM image of the InGaAs and InP nanoridges (enlarged view shows the undercut formed in InP below InGaAs), (b) small window opened in SiN to form top contact after forming gate contact on the left, and (c) a final device structure with the top, gate, and ground contacts.

and form separate mesas including the active layers (Figure 2b). Third, a thick Si_xN_y layer was deposited by PECVD and patterned to make an opening on top of the mesas (Figure 2c), and the first InP layer of 100 nm was etched using hydrochloric acid (HCl) and phosphoric acid (H_3PO_4) mixed solutions at 0 °C. The mixed solution almost does not attack the $In_{0.53}Ga_{0.47}As$ layer. Because the $In_{0.53}Ga_{0.47}As$ nanoridges form along the $\langle 01\bar{1} \rangle$ direction on the (100) InP wafer, the wet etching of InP formed a strong undercut shape. Figure 2d shows the side view normal to the nanoridges. Fourthly, a thin layer of SiO_2 was deposited using PECVD as gate dielectric, and a thin layer of Ti and Au was deposited and patterned to form the gate contacts (Figure 2e). Because of the strong undercut and thin SiO_2 layer, the gate and top metal contact layers were electrically disconnected (Figure 2f). Next, a small channel was patterned on the top metal contact, and an opening was patterned to form ground contacts. RIE was used to etch through the Si_xN_y layer (Figure 2g). Lastly, a thick Ti/Au metal layer was deposited and patterned to generate the top, gate, and ground contacts (Figure 2h).

Figure 3 shows the optical microscope and SEM images of the device at major processing steps. Figure 3a is the SEM image of the uniform and periodic $In_{0.53}Ga_{0.47}As$ and InP nanoridges. The enlarged view shows the undercut formed in InP below $In_{0.53}Ga_{0.47}As$, as we expected. Figure 3b shows the optical image of Ti/Au gate contact and the small channel opened in the Si_xN_y layer for forming the top contact, and Figure 3c shows the final device structure with top, gate, and ground contacts. After the above microfabrication steps, the back side of the sample was polished and the contacts were wire-bonded.

RESULTS AND DISCUSSION

The transport property of the device was measured in a temperature-controlled optical cryostat cooled with liquid nitrogen. Figure 4 shows the typical dark current curves at different temperatures. Multiple

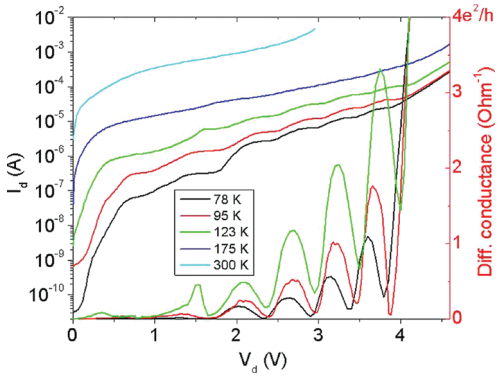

Figure 4. Measured dark current-bias curves for five different temperatures from 78 to 300 K and differential conductance curves for 78, 95, and 123 K.

current plateaus are observed when the bias increases from 78 K up to 123 K. Above 123 K, these oscillations were masked by the large thermionic dark current. In the same figure, we also plotted the differential conductance curves of the device for the first three temperatures. A few strong conductance oscillation peaks have been observed. These oscillation peaks appear in a quasi-periodic fashion, and the peak-to-valley ratios are almost an order high. The voltage separations between the adjacent peaks are between ~0.4 and ~0.9 V, which are much larger than the conduction band offset of $In_{0.53}Ga_{0.47}As$ and InP QWs (~0.242 eV). Therefore, sequential tunneling[30] between the ground and bound states could not be responsible. Besides, the thickness of our quantum barriers is 50 nm, too thick for sequential tunneling (for example, barriers are ~12 nm in ref 30). We believe these strong conductance oscillations originate from the resonant tunneling of the electrons through the energy states in all quantum wells produced by the lateral confinement. To confirm this, we simulated the dark current for the electrical confined quantum wells. In our model, we consider the dark current consisted of two parts, the thermionic and resonant tunneling current.[31] The calculations of both currents are shown

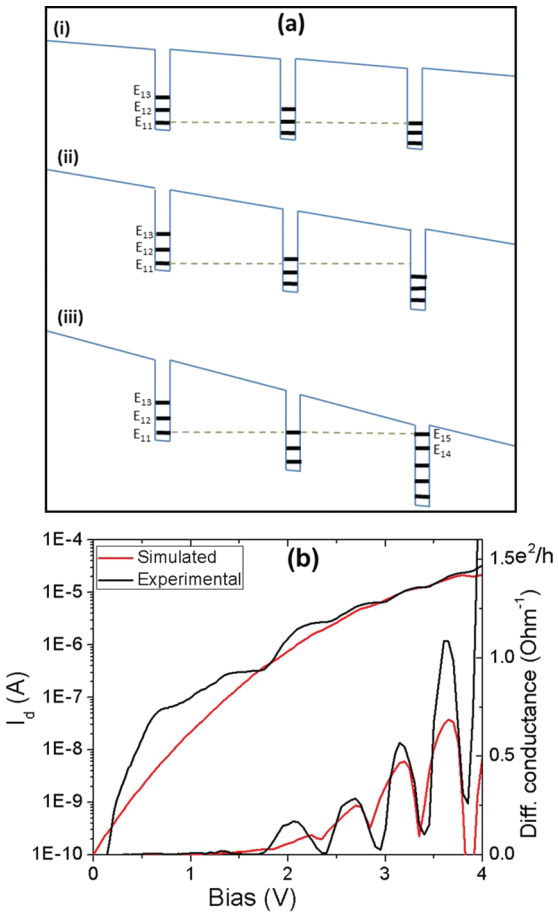

Figure 5. (a) Schematics of the aligned energy states at different biases increasing from (i) to (iii); (b) comparisons of the experimental and simulated dark current and differential conductance curves at 78 K.

in formulas 1 and 2.

$$I_{th} = \frac{e^2 m^*}{\pi\hbar^2}\frac{L_x}{n_y r} v_D t V \exp[-(H - E_i - E_f)/kT] \quad (1)$$

$$I_{tun} = \frac{eA}{\hbar L^2} D_1 D_2 kT \quad (2)$$

In the equations, e is the electronic charge, m^* is the effective mass of InGaAs, L_x is the length of the active region, v_D is the drift velocity of the carriers, t is the quantum mechanical transmission coefficient of an electron near the top of the barrier, V is the average potential drop per period, H is the barrier height, E_i is the energy of the ith sublevel, E_f is the temperature-dependent Fermi energy, k is the Boltzmann constant, T is the temperature, n_y is the number of the states per length in the lateral direction, r is the ratio of the gate to the ridge width, A is the area, and D_1 and D_2 are the tunneling coefficients for two consecutive quantum wells which are obtained using superposition of Lorentz functions centered at lateral energy eigenvalues. Strong tunneling current and differential conduction oscillations appear when the energy states in different quantum wells align with each other as the bias increases. Figure 5a illustrates the band diagram of three typical quantum wells with three different biases: (i), (ii), and (iii). The near-parabolic potential induced by the lateral electric field leads to almost equal separations between the energy levels. Considering the electrons' lifetime scattering, broadening of each energy state for quantum wires, and inhomogeneous broadening due to the nonuniformity of the electrical confinement at different depths, a broad resonant tunneling current is expected for each peak. If we add the resonant tunneling current with the thermionic one, multiple current steps and conductance oscillations appear. Figure 5b shows the simulated curve compared with the experimental one. The resonant tunneling coefficients and broadening width were fitted in the formulas above since there were no such experimental values.

The optical spectra of the device were also measured, and Figure 6a shows the normal-incident photocurrent response from the back side of the wafer at the bias of 1.25 V at 78 K for different gate voltages of 0, −1.5, and −3 V. With a more negative gate voltage, the peak responses get smaller and they shift to a longer wavelength (red-shift). This is because the photocurrent is primarily from optical excitation of electrons from lower to quasi-bond upper states in the well. With a stronger lateral electrical confinement, the energy of the lower states increases[32] and the difference between the lower and upper states is reduced, which produces a net red-shift in the photoresponse. In parallel, the increased depletion of the lower states leads to a reduced photocurrent. To confirm this, we used a finite-element method approach to model the potential distribution through the device and then numerically calculated the quantized energy levels in the nanowires. We then calculated the transfer matrix elements and the absorption spectra for the quantum wires as a function of the gate voltages. Figure 6b shows this simulation for three gate voltages, with a clear red-shift of the peak wavelengths at ∼8 μm. The electric field component in the quantum well growth direction was generated from the normal incident infrared light because the nonuniform gate metal surface produces a plasmonic effect[33] and induces the electric field component. Figure 6c shows the radial electrical potentials in the middle of the quantum wells at different gate voltages, and Figure 6d shows the simulated typical wave functions of the QWRs. The spacing between the ground and the first excited states due to the lateral electrical confinement is about 16 meV at a gate voltage of −3 V, which is significantly larger than the thermal energy at liquid nitrogen temperature ($kT \approx 6.7$ meV). Achieving a similar confinement

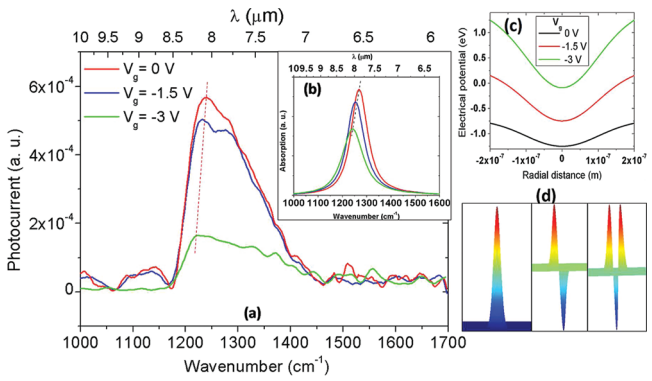

Figure 6. Measured photocurrent spectra of the QWR device at 78 K with different gate voltages. Inset (b) shows the simulated optical absorption spectra for different gate voltages. (c) Simulated electrical potential distribution *versus* different gate voltages V_g. (d) Typical electron wave functions for the nanowire.

using size-induced methods (*e.g.*, etching and regrowth) requires the lateral dimension of the quantum structures to be as small as ~30 nm.[34,35]

CONCLUSIONS

We report the fabrication and characterizations of novel electrically confined quantum wire stacks over large areas. Multiple current plateaus and conduction oscillations at above liquid nitrogen temperatures were observed due to the electrical confinement. The gate effect on the photoresponse of the detector was measured and compared with the theoretical prediction. This study demonstrates that strong lateral confinement could be utilized to produce stacks of nanowires, and potentially quantum dots, for optoelectronics applications.

Acknowledgment. This work was partially supported by the National Science Foundation under Grant No. ECCS-0621887. We acknowledge the use of electron beam lithography at Argonne National Laboratory's Center for Nanoscale Materials under the help of Dr. L. Ocola. Use of the Center for Nanoscale Materials was supported by the U.S. Department of Energy, Office of Science, Office of Basic Energy Sciences, under Contract No. DE-AC02-06CH11357. We are also grateful to the Materials Processing and Crystal Growth Facility and NUANCE facility at Northwestern University for fabrication and SEM characterizations.

REFERENCES AND NOTES

1. Barnham, K.; Vvedensky, D. *Low-Dimensional Semiconductor Structures: Fundamentals and Device Applications*; Cambridge University Press: Cambridge, 2001.
2. Park, J.; Pasupathy, A. N.; Goldsmith, J. I.; Chang, C.; Yaish, Y.; Petta, J. R.; Rinkoski, M.; Sethna, J. P.; Abruna, H. D.; McEuen, P. L.; *et al.* Coulomb Blockade and the Kondo Effect in Single-Atom Transistors. *Nature* **2002**, *417*, 722–725.
3. Komnik, A.; Gogolin, A. O. Resonant Tunneling between Luttinger Liquids: a Solvable Case. *Phys. Rev. Lett.* **2003**, *90*, 246403-1–4.
4. Beton, P. H.; Buhmann, H.; Eaves, L.; Foster, T. J.; Geim, A. K.; Scala, N. L.; Main, P. C.; Mansouri, L; Mori, N.; Sakai, J. W.; *et al*. Resonant Tunneling Quantum Dots and Wires: Some Recent Problems and Progress. *Semicond. Sci. Technol.* **1994**, *9*, 1912–1918.
5. Krive, I. V.; Palevski, A.; Shekhter, R. I.; Johson, M. Resonant Tunneling of Electrons in Quantum Wires. *Low Temp. Phys.* **2010**, *36*, 119–141.
6. Li, X.; Nakayama, H.; Yasuhiko, A. Phonon Bottleneck in Quantum Dots: Role of Lifetime of the Confined Optical Phonons. *Phys. Rev. B* **1999**, *59*, 5069–5093.
7. Nozik, A. J. Spectroscopy and Hot Electron Relaxation Dynamics in Semiconductor Quantum Wells and Quantum Dots. *Annu. Rev. Phys. Chem.* **2001**, *52*, 193–231.
8. Li, Y.; Qian, F.; Xiang, J.; Lieber, C. M. Nanowire Electronic and Optoelectronic Devices. *Mater. Today* **2006**, *9*, 18–27.
9. Wade, A.; Fedorov, G.; Smirnov, D.; Kumar, S.; Williams, B. S.; Hu, Q.; Reno, J. L. Magnetic-Field-Assisted Terahertz Quantum Cascade Laser Operating up to 225 K. *Nat. Photon.* **2009**, *3*, 41–45.
10. Minot, E. D.; Kelkensberg, F.; Kouwen, M. V.; Van Dam, J. A.; Kouwenhoven, L. P.; Zwiller, V.; Borgstrom, M. T.; Wunnicke, O.; Verheijen, M. A.; Bakkers, E. P. A. M. Single Quantum Dot Nanowire LEDs. *Nano Lett.* **2007**, *7*, 367–371.
11. Yan, R.; Gargas, D.; Yang, P. Nanowire Photonics. *Nat. Photon.* **2009**, *3*, 569–576.
12. Pettersson, H.; Tragardh, J.; Persson, A. I.; Landin, L.; Hessman, D.; Samuelson, L. Infrared Photodetectors in Heterostructure Nanowires. *Nano Lett.* **2006**, *6*, 229–232.
13. Zibik, E. A.; Grange, T.; Carpenter, B. A.; Porter, N. E.; Ferreira, R.; Bastard, G.; Stehr, D.; Winnerl, S.; Helm, M.; Liu H., Y.; *et al.* Long Lifetimes of Quantum-Dot Intersublevel Transitions in the Terahertz Range. *Nat. Mater.* **2009**, *8*, 803–807.
14. Asryan, L. V.; Luryi, S. Tunneling-Injection Quantum-Dot Laser: Ultrahigh Temperature Stability. *IEEE J. Quantum Electron.* **2001**, *37*, 905–910.
15. Wingreen, N. S.; Stafford, C. A. Quantum-Dot Cascade Laser: Proposal for an Ultralow-Threshold Semiconductor Laser. *IEEE J. Quantum Electron.* **2002**, *33*, 1170–1173.
16. Herrle, T.; Schmult, S.; Pindl, M.; Schwarz, U. T.; Wegscheider, W. T-Shaped Waveguides for Quantum-Wire Intersubband Lasers. *Phys. Rev. B* **2005**, *72*, 035316-1–7.
17. Das, B.; Singaraju, P. Novel Quantum Wire Infrared Photodetectors. *Infrared Phys. Technol.* **2005**, *46*, 209–218.
18. Tredicucci, A. Quantum Dots: Long Life in Zero Dimensions. *Nat. Mater.* **2009**, *8*, 775–776.
19. Zsebök, O.; Thordson, J. V.; Nilsson, B.; Andersson, T. G. Morphology of InGaAs/GaAs Quantum Wires Prepared by Highly Controlled Deep-Etching Techniques. *Nanotechnology* **2001**, *12*, 32–37.
20. Mu, X.; Ding, Y. J.; Yang, H.; Salamo, G. J. Vertically Stacking Self-Assembled Quantum Wires. *Appl. Phys. Lett.* **2002**, *81*, 1107–1109.
21. Bierwagen, O.; Masselink, W. T. Self-Organized Growth of InAs Quantum Wires and Dots on InP(001): the Role of Vicinal Substrates. *Appl. Phys. Lett.* **2005**, *86*, 113110–113110-3.
22. Elzerman, J. M.; Hanson, R.; Willems van Beveren, L. H.; Witkamp, B.; Vandersypen, L. M. K.; Kouwenhoven, L. P. Single-Shot Read-Out of an Individual Electron Spin in a Quantum Dot. *Nature* **2004**, *430*, 431–435.
23. Zheng, H. Z.; Wei, H. P.; Tsui, D. C. Gate-Controlled Transport in Narrow GaAs/$Al_xGa_{1-x}As$ Heterostructures. *Phys. Rev. B* **1986**, *34*, 5635–5638.
24. Sun, J.; Larsson, M.; Maximov, I.; Hardtdegen, H.; Xu, H. Q. Gate-Defined Quantum-Dot Devices Realized in InGaAs/

InP by Incorporating a HfO_2 Layer as Gate Dielectric. *Appl. Phys. Lett.* **2009**, *94*, 042114–6.
25. Cui, K.; Robinson, B. J.; Thompson, D. A.; Botton, G. A. Stacking Pattern of Multi-Layer InAs Quantum Wires Embedded in $In_{0.53}Ga_{0.47-x}Al_xAs$ Matrix Layers Grown Lattice-Matched on InP Substrate. *J. Cryst. Growth* **2010**, *312*, 2637–2646.
26. Simhony, S.; Kapon, E.; Colas, E.; Hwang, D. M.; Stoffel, N. G.; Worland, P. Vertically Stacked Multiple-Quantum-Wire Semiconductor Diode Lasers. *Appl. Phys. Lett.* **1991**, *59*, 2225–2227.
27. Williams, B. S. Terahertz Quantum-Cascade Lasers. *Nat. Photon.* **2007**, *1*, 517–525.
28. Bhattacharya, P.; Su, X.; Ariyawansa, G.; Perera, A. G. U. High-Temperature Tunneling Quantum-Dot Intersublevel Detectors for Mid-Infrared to Terahertz Frequencies. *Proc. IEEE* **2007**, *95*, 1828–1837.
29. Elias, P.; Kostic, I.; Soltys, J.; Hasenohrl, S. Wet-Etch Bulk Micromachining of (100) InP Substrates. *J. Micromech. Microeng.* **2004**, *14*, 1205–1214.
30. Han, Z. Y.; Yoon, S. F.; Radhakrishnan, K.; Zhang, D. H. Sequential Tunneling through N-Type GaAs/AlGaAs Multi-Quantum-Well Structures with Schottky and Ohmic Contacts. *J. Vac. Sci. Technol. B* **1995**, *13*, 4–9.
31. Choi, K. K.; Levine, B. F.; Malik, R. J.; Walker, J.; Bethea, C. G. Periodic Negative Conductance by Sequential Resonant Tunneling through an Expanding High-Field Superlattice Domain. *Phys. Rev. B* **1987**, *35*, 4172–4175.
32. Wu, W.; Dey, D.; Memis, O. G.; Mohseni, H. Modeling and Fabrication of Electrically Tunable Quantum Dot Intersubband Devices. *Appl. Phys. Lett.* **2009**, *94*, 193113–193113−3.
33. Wu, W.; Bonakdar, A.; Mohseni, H. Plasmonic Enhanced QWIP with High Detectivity. *Appl. Phys. Lett.* **2010**, *96*, 161107–161107−3.
34. Gossard, A. C.; Fafard, S. Quantum-Engineering of III-V Semiconductor Structures. *Solid State Commun.* **1994**, *92*, 63–70.
35. Kapon, E.; Hwang, D. M.; Walther, M.; Bhat, R.; Stoffel, N. G. Two-Dimensional Quantum Confinement in Multiple Quantum Wire Lasers Grown on OMCVD on V-Grooved Substrates. *Surf. Sci.* **1992**, *267*, 593–600.